small structures
www.small-structures.com

Long-Range Resonant Energy Transfer from Blue Thermally Activated Delayed Fluorescence Emitter to Red Quantum-Dot for Efficient Electroluminescence

Qiyin Chen, Jie Lin, Jingsong Huang, Wei Huang, and Guohua Xie**

Enhancing exciton utilization is crucial for boosting the performance of colloidal quantum-dot light-emitting diodes (QLEDs). The authors introduced a deep-blue thermally activated delayed fluorescence emitter, 10-(2,12-di-tert-butyl-5,9-dioxa-13b-boranaphtho(3,2,1-de)anthracen-7-yl)-9,9-dimethyl-9,10-dihydroacridine (TDBA-Ac), as a sensitizer doped in the hole transport layer to activate long-range resonant energy transfer to the quantum-dot-based emission layer. Photophysical and device characterization demonstrated that TDBA-AC can effectively harvest the excitons via reverse intersystem crossing and subsequently transfer the energy to the adjacent quantum-dot layer, thereby enhancing the utilization of excitons. A reduction of the hole injection barrier between the HTL and EML also achieves because of the deeper highest occupied molecular orbital of TDBA-Ac. As a result, the power efficiency and the external quantum efficiency of the sensitized red CdSe/ZnS QLEDs reach 42.8 lm W^{-1} and 26.9%, respectively, accompanied with a significantly low efficiency roll-off. The universality of this approach is also confirmed in the InP-based QLEDs.

1. Introduction

Colloidal quantum dot light-emitting diodes (QLEDs), recognized as one of the most advanced lighting and display technologies, have garnered significant attention and achieved remarkable progress over the last two decades.[1,2] This is largely due to its unique properties, such as solution-processability, high brightness, high efficiency, and superior color purity.[3,4] To construct high-performance QLEDs, inorganic metal oxide materials, like ZnO or ZnMgO, exhibiting high electron mobility, brilliant optical transparency, and good energy level alignment, are often used as the preferred electron transport layer (ETL).[5,6] For the hole transport layer (HTL), the most commonly used materials are polymers, e.g., poly((9,9-dioctylfluorenyl-2,7-diyl)-*co*-(4,4′-(N-(4-sec-butylphenyl)diphenylamine))) (TFB) and poly((9,9-dioctylfluorenyl-2,7-diyl)-alt-(9-(2-ethylhexyl)-carbazole-3,6-diyl)) (PF8Cz).[7,8] However, the mobilities of most HTLs are still much lower than those of ZnO and ZnMgO when used as the ETLs.[9,10] Additionally, the shallow highest occupied molecular orbitals (HOMOs) of these HTLs pose challenges for efficient hole injection due to the mismatched energy level alignment.[11] In such scenarios, imbalanced charge injection is an inevitable issue in QLEDs, which can readily result in excessive charge accumulation at the interface and undesirable non-radiative recombination.[1,12] This behavior significantly decreases the utilization of excitons and lowers the operational stability of the device.[2,13]

At present, researchers have not yet developed a sufficiently efficient material system to completely replace the commonly used organic HTLs in QLEDs and address the issue of unbalanced charge injection.[14–17] There are primarily two approaches to engineer the device structure for boosting the electroluminescent performance. The first approach is to reduce electron injection by altering the electrical properties of inorganic metal oxides or introducing an interface modification layer adjacent to the ETL. Alternatively, the other approach is to improve hole injection either through doping the HTL or employing a bilayer HTL structure.[18–21] For example, Tian's group doped ZnO with Mg^{2+} to decrease the electron mobility and match the hole mobility of the HTL; the optimized QLEDs exhibited a high external quantum efficiency (EQE) of 21.1% and a considerably low EQE roll-off.[22] Yang's group designed a stepwise bilayer structured HTL including the small molecule with the deep HOMO level to realize more efficient hole injection into QDs for improving the balance of charge injection in QLEDs. The resulting green device showed the significant efficiency enhancement and the lower

Q. Chen, W. Huang, G. Xie
Institute of Flexible Electronics (IFE, Future Technologies)
Future Display Institute of Xiamen, Tan Kah Kee Innovation Laboratory
Xiamen University
Xiamen 361102, China
E-mail: vc@nwpu.edu.cn; ifeghxie@xmu.edu.cn

Q. Chen, W. Huang, G. Xie
State Key Laboratory of Organic Electronics and Information Displays & Institute of Advanced Materials (IAM)
Nanjing University of Posts & Telecommunications
9 Wenyuan Road, Nanjing 210023, China

J. Lin, J. Huang
Oxford Suzhou Centre for Advanced Research (OSCAR)
University of Oxford
Suzhou 215123, China

The ORCID identification number(s) for the author(s) of this article can be found under https://doi.org/10.1002/sstr.202500503.

DOI: 10.1002/sstr.202500503

turn-on voltage (V_{on}), compared with the devices with the single-layer HTL.[23]

Recently, energy transfer incorporating the external sensitizers in QLEDs have been demonstrated to be useful.[24,25] For instance, the sensitizers doped in the HTL could transfer energy to the QD-based emitting layer (EML) via a nonradiative and long-range resonant energy transfer. This method could significantly reduce nonradiative recombination caused by charge accumulation and enhance exciton utilization.[26,27] For example, Cao's group realized efficient non-radiative energy transfer by employing blue phosphorescence dye bis[2-(4,6-difluorophenyl)pyridinato-C2, N](picolinato) iridium(III) (FIrpic) as a sensitizer in red QLEDs, resulting in a doubling of luminous efficiency.[28] Compared with the phosphorescent sensitizers, the thermally activated delayed fluorescence (TADF) ones function differently in QLEDs.[29] When incorporating the phosphorescent sensitizers, the triplet excitons participate in the non-radiative energy transfer due to intersystem crossing (ISC), which is usually related to Dexter energy transfer (DET) in a short transfer distance (several nm).[30] Conversely, for TADF sensitizers, roughly 100% of excitons can be converted into the singlets via reverse intersystem crossing (RISC); thus, long-range Förster resonance energy transfer (FRET) (about 10 nm) is projected to be the primary energy transfer pathway.[31] In the case of doping the sensitizers in the HTL, it would be more sufficient to use TADF materials with the extended exciton lifetime and bipolar charge transport to promote the energy transfer from the organic HTL to the QD-based EML.

In this contribution, a deep-blue TADF materials, 10-(2,12-di-tert-butyl-5,9-dioxa-13b-boranaphtho(3,2,1-de)anthracen-7-yl)-9,9-dimethyl-9,10-dihydroacridine (TDBA-Ac) with a high RISC rate constant of $9.9 \times 10^5\ s^{-1}$ and a long FRET radius of 7.8 nm, was incorporated into the HTL as the sensitizer to improve the performance of red QLEDs. The outstanding EQE of 26.9% and a relatively low EQE roll-off were demonstrated, due to the sufficiently enhanced exciton utilization and improved hole injection. Photoluminescence (PL) and time-resolved photoluminescence (TRPL) results indicated that TDBA-Ac could realize effective long-distance energy transfer. The transient electroluminescence (TREL) and capacitance-voltage (C-V) confirmed the minimized nonradiative recombination and thus improved exciton utilization.

2. Results and Discussion

As shown in **Figure 1**a, the deep-blue TADF dye TDBA-Ac with a rigid and symmetrical oxygen-bridged boron acceptor and dimethylacridine donor was selected as a sensitizer in this work. TDBA-Ac has a very small singlet-triplet energy gap of 0.06 eV, a high photoluminescence quantum yields (PLQY) of 93%, and a RISC rate constant of $9.9 \times 10^5\ s^{-1}$, which can efficiently convert triplet excitons into singlet excitons at room temperature.[32] The PL measurement revealed that TDBA-Ac exhibits deep-blue emission at 463 nm which significantly overlaps with the absorption spectrum of the CdSe/ZnS-based red QDs and the spectral overlap integral was determined to be $4.6 \times 10^{16}\ nm^4\ M^{-1}\ cm^{-1}$ (see Figure 1b), indicating the capacity of promoting FRET process from TDBA-Ac to QDs. The FRET radius (R_0) is defined and calculated as follows.[33,34]

$$R_0{}^6 = \frac{9000(\ln 10)\Phi_D \kappa^2}{128\pi^5 n^4 N_A} \int_0^\infty F_D(\lambda)\varepsilon_A(\lambda)\lambda^4 d\lambda \quad (1)$$

where Φ_D is the PLQY of the donor TDBA-Ac, κ^2 is a factor of the relative orientation of the transition dipoles of the donor TDBA-Ac and the acceptor QDs, assumed to be 2/3. n is the refractive index of the medium, assumed to be 1.7 here,[35] N_A is Avogadro's number, $F_D(\lambda)$ is the normalized emission spectra of donor TDBA-Ac, and $\varepsilon_A(\lambda)$ is the molar extinction coefficient of the acceptor QDs. From the equation, R_0 was calculated to be 7.9 nm, indicating that the donor TDBA-Ac can provide a long-range resonant energy transfer to the acceptor QDs.

Herein, we incorporated TDBA-Ac into TFB at various mass ratios: 0% (T0), 1% (T1), 2% (T2), and 5% (T5) as the HTLs, respectively. The PL measurements were performed to record the PL intensity of the QDs deposited onto these HTLs to investigate the effect of FRET. As shown in **Figure 2**a, the incorporation of TDBA-Ac led to a significant enhancement in the PL intensity of the QD-based EML, and this enhancement persistently increased

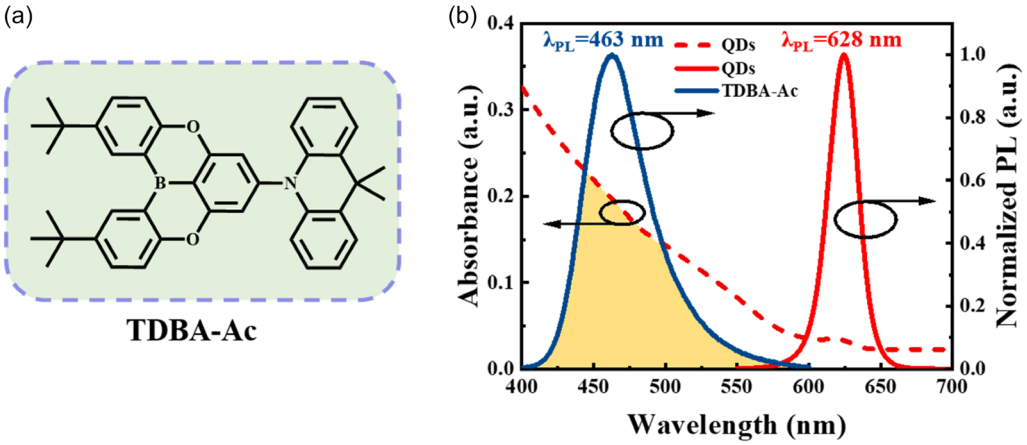

Figure 1. a) Chemical structure of TDBA-Ac. b) The absorption and normalized PL spectra of the CdSe/ZnS-based red QDs film, and the normalized PL spectrum of TDBA-Ac.

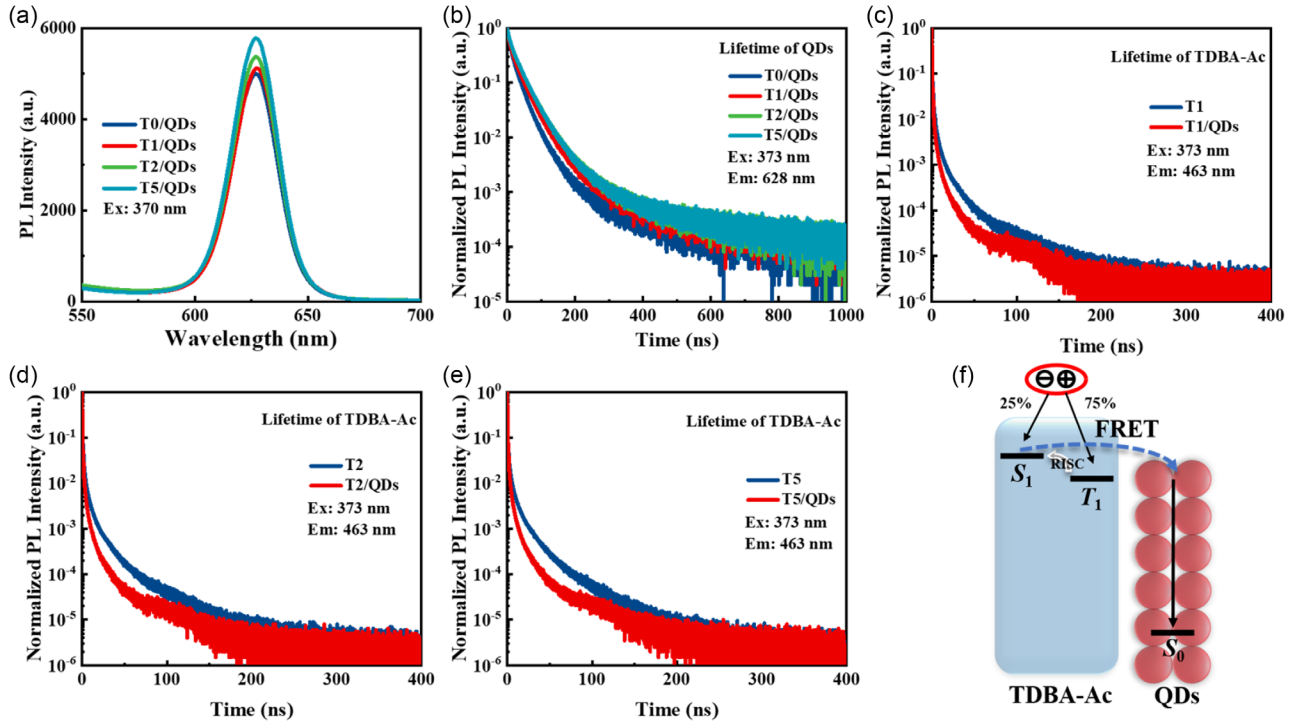

Figure 2. a) PL and b) TRPL spectra of the QDs films deposited on the T0, T1, T2, and T5 films measured at the wavelength of 628 nm, respectively. TRPL spectra measured at the peak emissive wavelength of TDBA-Ac (463 nm) for the single-layer c) T1, d) T2, and e) T5 films and the corresponding bilayer T1/QDs, T2/QDs, T5/QDs films, respectively. f) Schematic diagram of FRET process between TDBA-Ac in the HTL and QDs.

as the concentration of TDBA-Ac within HTLs was elevated. The PL results suggest that TDBA-Ac may potentially suppress the interface exciton quenching and/or facilitate the transfer of exciton energy from the HTL to the QDs. To further elucidate the role of TDBA-Ac, the transient photoluminescence (TRPL) was employed to record the average fluorescence lifetimes (τ_{avg}) of QDs and TDBA-Ac at the wavelengths of 628 and 463 nm, respectively. The TRPL spectra of QDs deposited on the four HTLs (namely, T0, T1, T2, and T5 films). As shown in Figure 2b, the rendered τ_{avg}s were 28.2, 32.4, 36.0, and 35.8 ns, respectively. The τ_{avg}s of QDs deposited on the HTLs with TDBA-Ac was respectively longer than those of QDs coated on the neat TFB film, indicating the additional energy transfer process at the presence of TDBA-Ac. Furthermore, the TRPL spectra of TDBA-Ac in the single-layer T1, T2, and T5 films and the bilayer films of T1/QDs, T2/QDs, and T5/QDs were respectively shown in Figure 2c–e. The τ_{avg}s are summarized in **Table 1**. It is evident that the τ_{avg} of TDBA-Ac decreased significantly when QDs were coated on the HTL. From these results, we can conclude that energy transfer occurs effectively from TDBA-Ac to QDs through the long-range FRET process.

Atomic force microscopy (AFM) was employed to determine the surface morphology of the T0, T1, T2, and T5 films, and the AFM images of the four films exhibited relatively low root mean square (RMS) roughness values of 0.25, 0.22, 0.25, and 0.28 nm (see Figure S1, Supporting Information), respectively. The consistent RMS values indicated that a low concentration of TDBA-Ac does not adversely affect the surface morphology of HTL film, while high content of TDBA-Ac may compromise the quality of HTL films due to the poor film-forming characteristics of small molecule materials.[36] In this case, we could find that the RMS of T5 film is higher than T0 film, which may result in an inferior interface in QLEDs.

Table 1. Comparison of the fluorescence lifetime of QDs (measured at 628 nm) and TDBA-Ac (measured at 463 nm) of T0/QDs, T1/QDs, T2/QDs, and T5/QDs bilayer films and T1, T2, and T5 single-layer films.

	Films						
	T0/QDs	T1	T1/QDs	T2	T2/QDs	T5	T5/QDs
QDs	28.2 ns	–	32.4 ns	–	36.0 ns	–	35.8 ns
TDBA-Ac	–	15.9 ns	13.9 ns	14.2 ns	11.5 ns	12.5 ns	10.5 ns

The effect of TDBA-Ac on the EL performance of QLEDs was evaluated by constructing the devices with the following structure: anode/hole injection layer (HIL)/HTL/EML/ETL/cathode. ITO and Al were used as anode and cathode, respectively. Specifically, PEDOT:PSS, T0, T1, T2, and T5 films, red CdSe/ZnS QDs, and ZnMgO NPs served as the HIL, HTL, EML, and ETL, respectively. The devices with T1, T2, and T5 films as the HTLs were named as HTL1, HTL2, and HTL5, respectively. The control device HTL0 with the T0 film (neat TFB) as the HTL was fabricated concurrently as the reference. The schematic diagram of the device structure is shown in **Figure 3**a.

From the current density–voltage–luminance (*J-V-L*) curves (Figure 3b), we observed that at low doping concentrations of TDBA-Ac in HTLs, the current density of HTL1 and HTL2

devices increased. However, upon reaching a concentration of 5%, the current density experienced a sudden decline, which implied that the elevated concentration of TDBA-Ac might potentially deteriorate the quality of the HTL film, as indicated by AFM measurement. This may consequently hamper the injection and transport of charge carriers. From the *J-V* curves of all four devices, we obtained the ideality factor by fitting them based on the diode model equation.[7]

$$J = J_0\left[\exp\left(\frac{qV}{nkT}\right) - 1\right] \tag{2}$$

where J is the current density, J_0 is the saturation dark current density, q is the elementary charge, V is the voltage, n is the ideality factor of device, k is the Boltzmann constant, and T is the room temperature in Kelvin (300 K).

The fitting results reveal that the ideality factors of the devices HTL1, HTL2, and HTL5 are 3.37, 3.44, and 4.26, respectively, while it is 4.88 for the control device HTL0. The lower ideality factor means better charge injection and transport. Since all devices share same electron injection, we infer that a low concentration TDBA-Ac enhances hole injection and transport, leading to more balanced charge injection within the device. However, when the concentration reaches 5%, the charge injection balance becomes worse again.

It is worth noting that, under the same driving voltage, the devices HTL1 and HTL2 exhibited a substantially higher brightness, compared with the control device HTL0. This indicates that TDBA-Ac can effectively ensure the energy transfer from HTL to QD-based EML. It is observed that the V_{on} of the device HTL5 increased, while the V_{on}s of the devices HTL1 and HTL2 were slightly lower, compared with that of the control device HTL0. These differences are likely due to changes in the electrical properties of the HTLs within the devices. Combined with the AFM analysis of the film morphology, it can be concluded that the concentration of TDBA-Ac in the HTLs would be the dominant factor.

Figure 3c,d indicated that the EL performance of the devices HTL1, HTL2, and HTL5 were significantly improved, compared

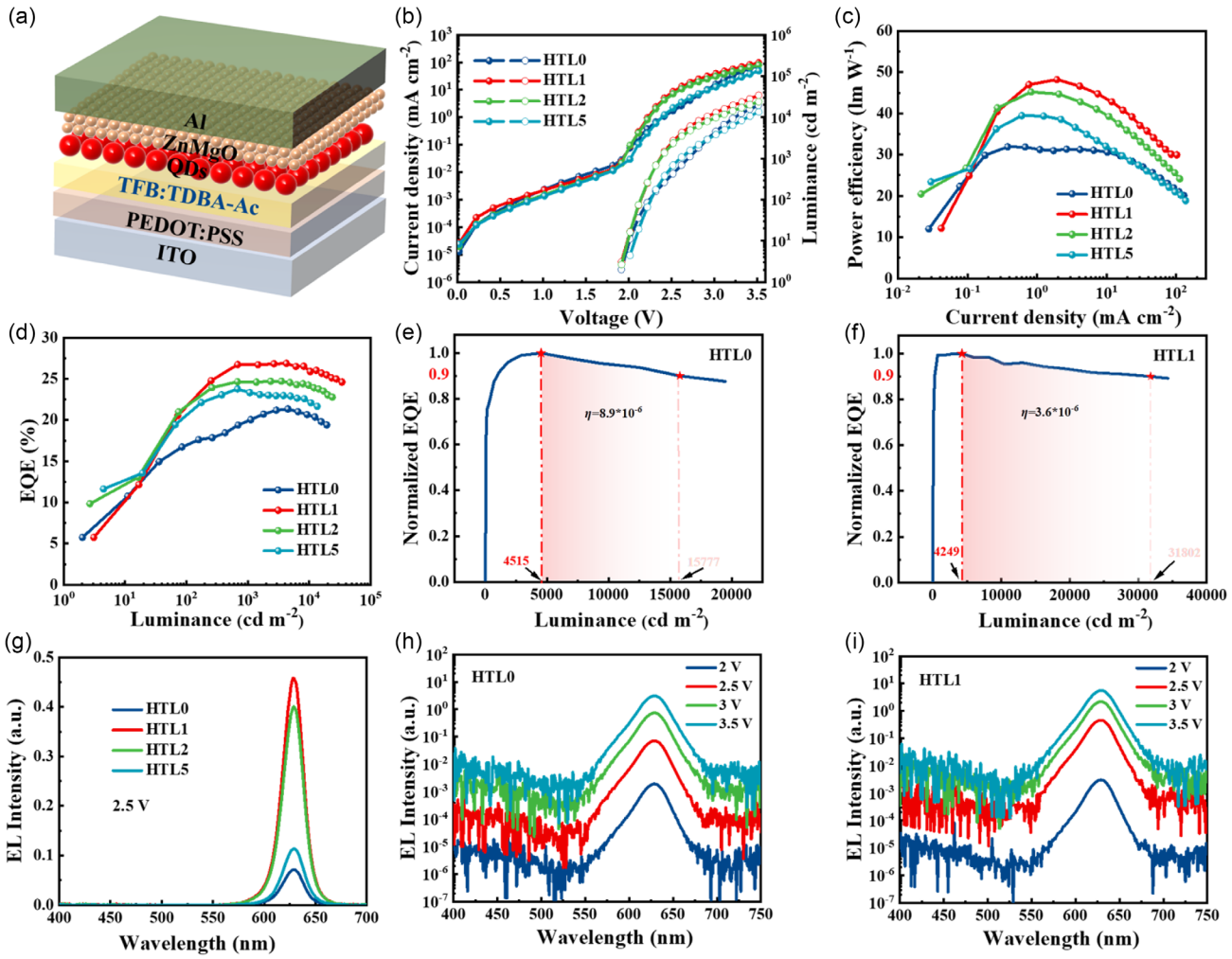

Figure 3. a) Schematic diagram of the device structure. b) *J-V-L*, c) PE, and d) EQE curves of the devices HTL0, HTL1, HTL2, and HTL5, respectively. Normalized EQE curves as a function of luminance of the devices e) HTL0 and f) HTL1, respectively. g) EL spectra of the devices HTL0, HTL1, HTL2, and HTL5 at 2.5 V. EL spectra of the devices h) HTL0 and i) HTL1 at different driving voltages, respectively.

Table 2. Comparison of the EL performance of the devices.

Devices	V_{on} [a] [V]	λ_{EL} [b] [nm]	FWHM [c] [nm]	PE [d] [lm W^{-1}]	CE [e] [cd A^{-1}]	EQE [f] [%]	CIE [g] (x, y)
HTL0	2.01	628	24.7	29.7	28.5	21.3	(0.68,0.31)
HTL1	1.99	628	24.5	42.8	35.7	26.9	(0.68,0.31)
HTL2	1.99	628	24.6	41.0	32.9	24.7	(0.68,0.31)
HTL5	2.07	628	25.4	38.6	30.9	23.8	(0.68,0.31)

[a]Turn-on voltage at a luminance of 10 cd m^{-2}. [b]Peak wavelength of the EL spectrum. [c]Full-width at half-maximum of the EL spectrum. [d]Maximum power efficiency. [e]Maximum current efficiency. [f]Maximum external quantum efficiency. [g]Commission International de l'Eclairage color coordinates.

with that of the control device HTL0. For instance, the EQE of the device HTL1 increased 26.9% (21.3% for the control device HTL0). Its power efficiency (PE) and current efficiency (CE) both rose from 29.7 lm W^{-1} and 28.5 cd A^{-1} to 42.8 lm W^{-1} and 35.7 cd A^{-1}, respectively (**Table 2**). These values represent the best performance among the four devices. Additionally, Figure 3e,f clearly showed that the EQE roll-off of the device HTL1 was significantly lower than that of the control device HTL0. When the brightness reached ≈10 000 cd m^{-2}, the EQE of the device HTL0 rapidly decreased by about 10%, dropping down to 19.2%. In contrast, the device HTL1 reached a peak EQE of 26.9% at a brightness of 4249 cd m^{-2} and experienced an efficiency roll-off of ≈ 10% until the brightness increased to 31 802 cd m^{-2} with an EQE of 24.2%. A factor η is introduced to clearly quantify the efficiency roll-off behavior, which is defined as $\eta = 10\%/\Delta L$. Here, 10% corresponds to the reduction in EQE from its maximum value to 90%, and ΔL represents the associated change in luminance. A lower value of η indicates a reduced efficiency roll-off. In this case, the η values for the devices HTL0 and HTL1 are calculated as 8.9×10^{-6} and 3.6×10^{-6}, respectively, demonstrating that significantly suppressed efficiency roll-off in the device HTL1. The devices HTL2 and HTL5 also exhibited the alleviated EQE roll-offs (see Figure S2, Supporting Information). This reduction in the EQE roll-off strongly illustrates that TDBA-Ac not only promote energy transfer to the QD-based EML but also reduce the exciton quenching.

To determine whether TDBA-Ac produced the residual emission which would sacrifice the color purity, we analyzed the EL spectra of all four devices. Notably, as depicted in Figure 3g, no emission bands were observed in the blue range for any devices, regardless of the concentration of TDBA-Ac in HTLs. The EL spectra indicated that TDBA-Ac does not emit when subjected to an electric field. Furthermore, we examined the EL spectra of the four devices under various driving voltages from 2 to 3.5 V (see Figure 3h,i and Figure S3, Supporting Information). No any residual blue emission was detectable. Additionally, across all devices, the emission peaks were consistently located at 628 nm with a full width at half maximum (FWHM) of ≈25 nm (Table 2), corresponding to the Commission Internationale de l'Éclairage (CIE) color coordinates of (0.68, 0.31).

Time-resolved electroluminescence (TREL) measurement was conducted to elucidate the influence of TDBA-Ac on charge carrier and exciton dynamics within the devices HTL0 and HTL1. **Figure 4**a illustrates the rising part curves of the devices under a pulsed voltage of 3 V. Given that the electron transport is identical across all devices, the differences in the switch-on time of the EL intensity are likely due to the difference in hole transport. It was observed that the switch-on time for the devices HTL0 and HTL1 remained almost consistent, indicating a low concentration of TDBA-Ac that has a neglectable impact on hole transport. As shown in Figure 4b, the decay lifetimes of the devices HTL0 and HTL1 were determined by fitting the curves using a double exponential fitting formula, i.e., 4.43 and 1.77 µs, respectively. Notably, the exciton lifetime of the device HTL1 was significantly shorter than that of the control device HTL0, indicating the faster exciton recombination in the sensitized devices, compared with the control device. This observation suggests that TDBA-Ac can efficiently utilize exciton energy and facilitate radiative recombination.

It is crucial to understand the impact of TDBA-Ac on the carrier transport behavior in devices, we utilized impedance spectroscopy (IS) to measure the resistance of the devices HTL0 and HTL1, shown in Figure 4c. Since the other layers were identical, we believe that the changes observed in the QLEDs were induced mainly by TDBA-Ac. It is clear that the device with the doped HTL exhibited the lower resistance and thus achieved more efficient charge transport.

Also, ultraviolet photoelectron spectroscopy (UPS) was conducted to measure the energy levels of the films T0 and T1 (see Figure S4, Supporting Information). The HOMO levels of both films were determined to be –5.36 and –5.41 eV, respectively. The lower energy level means that TDBA-Ac can also reduce the hole injection barrier. Therefore, these results directly suggest that a low concentration of TDBA-Ac is beneficial to hole injection.

To further investigate the role of TDBA-Ac in carrier injection, we examined the capacitance-voltage (*C-V*) characteristics of the devices HTL0 and HTL1 at a fixed frequency of 10 kHz, as shown in Figure 4d. At bias voltages below 0.5 V, the geometric capacitance values of the two devices reCmain almost constant at 2.6 nF, indicating that TDBA-Ac has negligible impact on the HTL thickness. This observation agreed well with the measured thickness of each film (see Figure S5, Supporting Information). Additionally, the capacitance at over 2.5 V of the devices HTL1 was lower than that of the control device HTL0. This indicates the faster radiative recombination within the EML. These results further confirm that TDBA-Ac possesses the ability to facilitate the hole injection/transport and decrease charge accumulation.

The universality of the energy transfer strategy across different QD systems is essential. To this end, we extended this strategy to red InP-based QLEDs by simply changing the QDs from CdSe/ZnS to InP system. The EL performance of the InP devices were illustrated in Figure S6 and Table S1, Supporting Information. Similarly, the EL performance of the sensitized device significantly outperforms the control device. For instance, the EQE of the device with 1 wt% TDBA-Ac increased from 6.6% to 9.0%, compared with the control device, and the V_{on} of the device concurrently decreased. These outcomes from the red InP-based QLED further validate the universality of TDBA-Ac as a sensitizer for long-range resonant energy transfer.

Based on the aforementioned characterizations and analysis, as shown in **Figure 5**, we can deduce that TDBA-Ac as

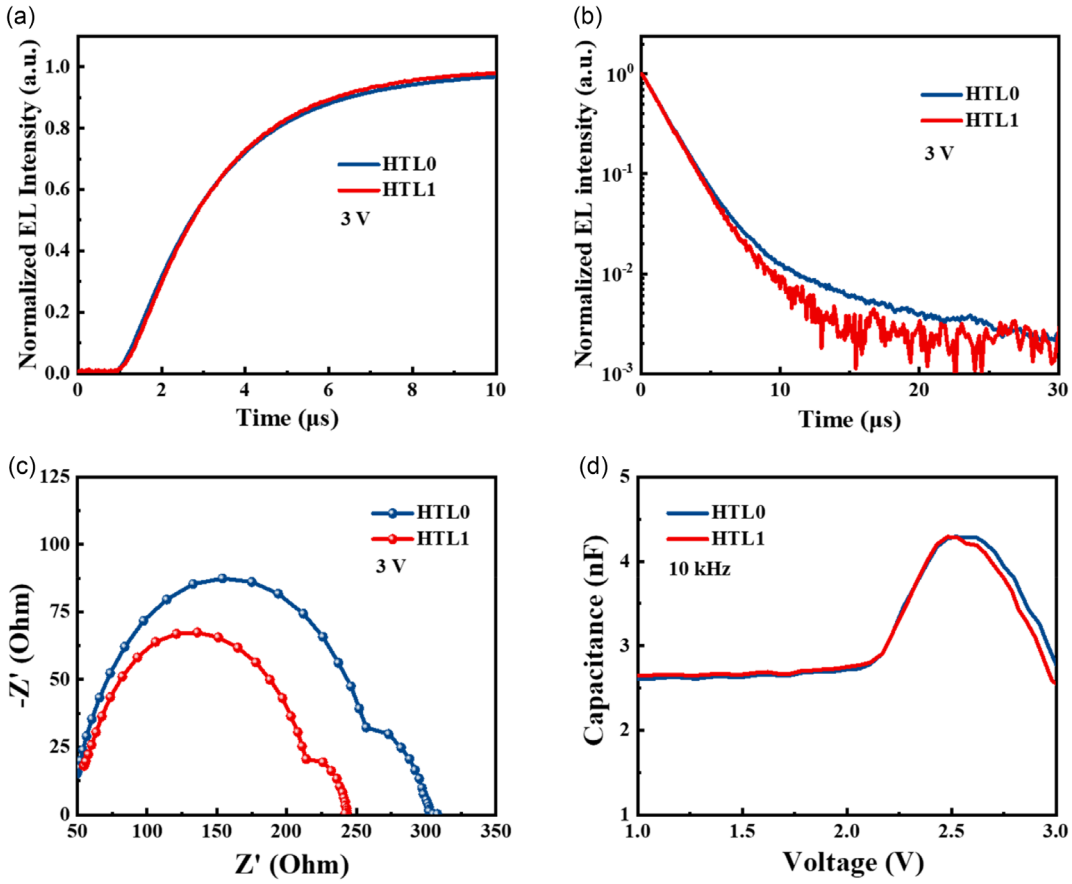

Figure 4. The a) rising and b) decay parts of the TREL curves of the devices HTL0 and HTL1 at a pulsed voltage of 3 V, respectively. c) Impedance curves at 3 V, d) *C-V* curves at a fixed frequency of 10 kHz.

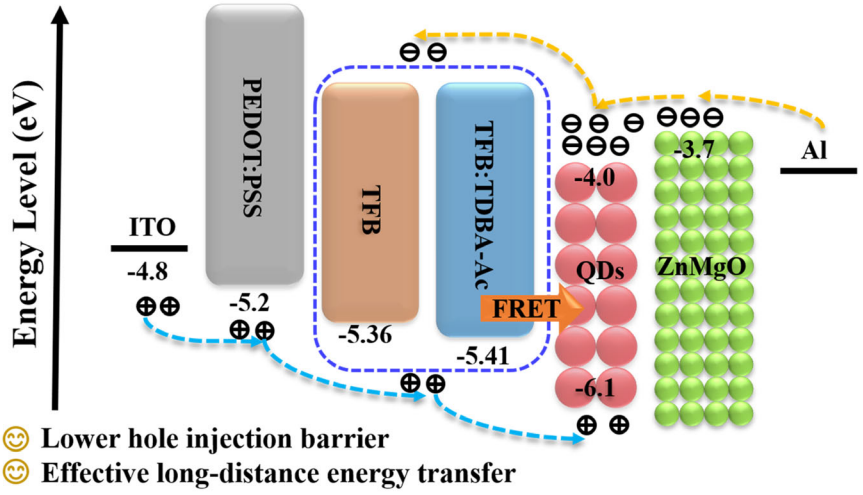

Figure 5. Schematic diagrams of energy level alignment of the device and FRET process from TDBA-Ac to QDs EML.

a sensitizer is not only effective in improving the exciton utilization but also powerful in reducing the hole injection barrier. These factors play a vital role in boosting EL performance.

3. Conclusions

In summary, highly efficient red QLEDs with the low EQE roll-off were successfully demonstrated by introducing the thermally

activated delayed fluorescence materials TDBA-Ac as a sensitizer to trigger long-range resonant energy transfer. The characterizations of photophysics and devices clarify that TDBA-Ac plays a vital role in enhancing exciton utilization and improving holes injection, simultaneously. As a result, the sensitized device achieved an unprecedentedly high PE of 42.8 lm W^{-1} and high EQE of 26.9% with the alleviated efficiency roll-off, and the universality of the strategy was also testified. The in-depth understanding of the long-range resonant energy transfer strategy in QLEDs will offer a robust method for boosting the overall EL performance.

Supporting Information

Supporting Information is available from the Wiley Online Library or from the author.

Acknowledgements

This work was supported by the National Key R&D Program of China (no. 2024YFB3612604) and the National Natural Science Foundation of China (nos. 52373195 and 62175189). G.X. acknowledged the funding support from the Key Science and Technology Project on Future Industries of Xiamen City (no. 3502Z20231052), the Opening Project of Key Laboratory of Optoelectronic Chemical Materials and Devices, Ministry of Education, Jianghan University (no. JDGD-202301), and the Open Research Fund of State Key Laboratory of Organic Electronics and Information Displays.

Conflict of Interest

The authors declare no conflict of interest.

Author Contributions

Qiyin Chen: data curation (lead); formal analysis (lead); investigation (lead). **Jie lin**: investigation (supporting); methodology (supporting); and software (equal). **Jingsong Huang**: investigation (supporting); project administration (supporting); and supervision (equal). **Wei Huang**: funding acquisition (equal); project administration (equal); and supervision (equal). **Guohua Xie**: conceptualization (lead); funding acquisition (lead); investigation (equal); project administration (lead); and supervision (lead).

Data Availability Statement

The data that support the findings of this study are available from the corresponding author upon reasonable request.

Keywords

energy transfer, exciton utilization, quantum dots, sensitizer, thermally activated delayed fluorescence

Received: July 29, 2025
Revised: September 12, 2025
Published online:

[1] Z. A. Chen, H. T. Li, C. X. Yuan, P. L. Gao, Q. Su, S. M. Chen, *Small Methods* **2024**, *8*, 2300359.
[2] D. Tian, H. Ma, G. Huang, M. Gao, F. Cai, Y. Fang, C. Li, X. Jiang, A. Wang, S. Wang, Z. Du, *Adv. Opt. Mater.* **2023**, *11*, 2201965.
[3] E. Jang, H. Jang, *Chem. Rev.* **2023**, *123*, 4663.
[4] X. Liu, F. Liu, K. Wu, H. Li, *The Innovation Mater.* **2025**, *3*, 100124.
[5] S.-Y. Yoon, Y.-J. Lee, H. Yang, D.-Y. Jo, H.-M. Kim, Y. Kim, S. M. Park, S. Park, H. Yang, *ACS Energy Lett.* **2022**, *7*, 2247.
[6] J. Pan, J. Chen, Q. Huang, Q. Khan, X. Liu, Z. Tao, Z. Zhang, W. Lei, A. Nathan, *ACS Photonics* **2016**, *3*, 215.
[7] Q. Chen, Y. Hu, J. Lin, J. Huang, S.-L. Gong, G. Xie, *Nanoscale Horiz.* **2024**, *9*, 465.
[8] Y. Deng, F. Peng, Y. Lu, X. Zhu, W. Jin, J. Qiu, J. Dong, Y. Hao, D. Di, Y. Gao, T. Sun, M. Zhang, F. Liu, L. Wang, L. Ying, F. Huang, Y. Jin, *Nat. Photonics* **2022**, *16*, 505.
[9] W. Wu, Z. Chen, Y. Zhan, B. Liu, W. Song, Y. Guo, J. Yan, X. Yang, Z. Zhou, W.-Y. Wong, *Adv. Mater. Interfaces* **2021**, *8*, 2100731.
[10] X. Jin, C. Chang, W. Zhao, S. Huang, X. Gu, Q. Zhang, F. Li, Y. Zhang, Q. Li, *ACS Appl. Mater. Interfaces* **2018**, *10*, 15803.
[11] W. Wang, Q. Chen, G. Hua, J. Lin, J. Huang, G. Xie, W. Tang, *The Innovation Mater.* **2025**, *3*, 100151.
[12] Q. Yuan, T. Wang, P. Yu, H. Zhang, H. Zhang, W. Ji, *Org. Electron.* **2021**, *90*, 106086.
[13] J. H. Chang, P. Park, H. Jung, B. G. Jeong, D. Hahm, G. Nagamine, J. Ko, J. Cho, L. A. Padilha, D. C. Lee, C. Lee, K. Char, W. K. Bae, *ACS Nano* **2018**, *12*, 10231.
[14] C. Cheng, A. Liu, G. Ba, I. S. Mukhin, F. Huang, R. M. Islamova, W. C. H. Choy, J. Tian, *J. Mater. Chem. C* **2022**, *10*,15200.
[15] S. Lei, Y. Xiao, K. Yu, B. Xiao, M. Wan, L. Zou, Q. You, R. Yang, *Adv. Funct. Mater.* **2023**, *33*, 2305732.
[16] J. Kim, J. Roh, M. Park, C. Lee, *Adv. Mater.* **2024**, *36*, 2212220.
[17] S. Rhee, K. Kim, J. Roh, J. Kwak, *Curr. Opt. Photon.* **2020**, *4*, 161.
[18] T. Wang, L. Xie, F. Su, X. Meng, Y. Song, W. Su, Z. Cui, *Nanoscale* **2023**, *15*, 18523.
[19] J. Jing, L. Lin, K. Yang, H. Hu, T. Guo, F. Li, *Org. Electron.* **2022**, *103*, 106466.
[20] Z. Luo, Y. Yu, K. Yang, L. Lin, J. Lin, T. Guo, H. Hu, F. Li, *Adv. Electron. Mater.* **2023**, *9*, 2200970.
[21] D. Chen, D. Chen, X. Dai, Z. Zhang, J. Lin, Y. Deng, Y. Hao, C. Zhang, H. Zhu, F. Gao, Y. Jin, *Adv. Mater.* **2020**, *32*, 2006178.
[22] C. Cheng, X. Sun, Z. Yao, C. Bi, X. Wei, J. Wang, J. Tian, *Sci. China Mater.* **2022**, *65*, 1882.
[23] X. Wang, P. Shen, F. Cao, S. Wang, H. Wang, Q. Wu, J. Zhang, X. Yang, *IEEE Electron Device Lett.* **2019**, *40*, 1139.
[24] Y. Wang, Y. Yang, D. Zhang, T. Zhang, S. Xie, Y. Zhang, Y.-B. Zhao, X. Mi, X. Liu, *Adv. Mater.* **2023**, *35*, 2306703.
[25] W. Zheng, D. Song, S. Zhao, B. Qiao, Z. Xu, J. Chen, P. Wang, Y. Liang, *Org. Electron.* **2020**, *77*, 105544.
[26] Z. Zhang, X. Guan, Z. Kang, H. Zhang, Q. Zeng, R. Yu, R. Wang, W. Ji, *Org. Electron.* **2019**, *73*, 337.
[27] Y.-N. Zhang, Y.-S. Liu, M.-M. Yan, Y. Wei, Q.-L. Zhang, Y. Zhang, *ACS Appl. Mater. Interfaces* **2018**, *10*, 7435.
[28] L. Lan, B. Liu, H. Tao, J. Zou, C. Jiang, M. Xu, L. Wang, J. Peng, Y. Cao, *J. Mater. Chem. C* **2019**, *7*, 5755.
[29] J. Kim, A. Hong, D. Hahm, H. Lee, W. K. Bae, T. Lee, J. Kwak, *Adv. Opt. Mater.* **2023**, *11*, 2300088.
[30] R. Lai, Y. Liu, X. Luo, L. Chen, Y. Han, M. Lv, G. Liang, J. Chen, C. Zhang, D. Di, G. D. Scholes, F. N. Castellano, K. Wu, *Nat. Commun.* **2021**, *12*, 1532.
[31] K. Goushi, K. Yoshida, K. Sato, C. Adachi, *Nat. Photonics* **2012**, *6*, 253.
[32] D. H. Ahn, S. W. Kim, H. Lee, I. J. Ko, D. Karthik, J. Y. Lee, J. H. Kwon, *Nat. Photonics* **2019**, *13*, 540.

[33] Y. Tang, Y. Liu, W. Ning, L. Zhan, J. Ding, M. Yu, H. Liu, Y. Gao, G. Xie, C. Yang, *J. Mater. Chem. C* **2022**, *10*, 4637.
[34] S. Melle, O. G. Calderón, M. Laurenti, D. Mendez-Gonzalez, A. Egatz-Gómez, E. López-Cabarcos, E. Cabrera-Granado, E. Díaz, J. Rubio-Retama, *J. Phys. Chem. C* **2018**, *122*, 18751.
[35] P. Wei, D. Zhang, L. Duan, *Adv. Funct. Mater.* **2020**, *30*, 1907083.
[36] L. Chen, C. Zhang, G. Lin, H. Nie, W. Luo, Z. Zhuang, S. Ding, R. Hu, S.-J. Su, F. Huang, A. Qin, Z. Zhao, B. Z. Tang, *J. Mater. Chem. C* **2016**, *4*, 2775.